STAP REVIEW

Advanced capacitor technology based on two-dimensional nanosheets

To cite this article: Hyung-Jun Kim *et al* 2016 *Jpn. J. Appl. Phys.* **55** 1102A3

View the article online for updates and enhancements.

Japanese Journal of Applied Physics **55**, 1102A3 (2016)
http://doi.org/10.7567/JJAP.55.1102A3

STAP REVIEW

Nanoarchitectonics for manipulation of atom, molecule, and materials

Advanced capacitor technology based on two-dimensional nanosheets

Hyung-Jun Kim, Minoru Osada*, and Takayoshi Sasaki

International Center for Materials Nanoarchitectonics (WPI-MANA), National Institute for Materials Science (NIMS), Tsukuba, Ibaraki 305-0044, Japan

*E-mail: osada.minoru@nims.go.jp

Received June 14, 2016; accepted July 6, 2016; published online September 8, 2016

As electronics continue to decrease in size, new classes of materials are necessary to continue this downsizing trend. Of particular importance is the development of high-performance capacitors based on dielectric films. Ultrathin high-*k* dielectrics are expected to be key to future applications. Recently, we have developed new high-*k* nanodielectrics based on molecularly thin oxide nanosheets [$Ti_{0.87}O_2$, Ti_2NbO_7, $(Ca,Sr)_2Nb_3O_{10}$]. Newly developed nanosheets exhibited the highest permittivity ($\varepsilon_r > 100$) ever realized in all known dielectrics in the ultrathin region (<10 nm). In this review, we present recent progress in dielectric nanosheets, highlighting emerging functionalities in capacitor applications.

1. Introduction

Capacitors are ubiquitous in electronic devices and systems. Because capacitors are the largest elements in current electronic devices, increasing their capacitance in smaller areas/volumes is an important step for the relentless advances in microelectronic technologies. So far, the miniaturization of capacitor components has been accomplished through new materials and fabrication technologies, e.g., adoption of high-*k* materials, thinning of the dielectric layer, and multilayer implementation in multilayer ceramic capacitors (MLCCs).[1–4] $BaTiO_3$ (BT) is one of the most important dielectric materials widely used for MLCCs. State-of-the-art MLCC technology now enables the fabrication of the multilayer structure with a thin BT ceramic layer (500 nm) using ~100 nm size particles. Future advances in MLCCs require the integration of thinner dielectric layers, but the formidable challenge lies in so-called size effects.[5,6] As the size of BT particles decreases to below 100 nm, BT particles yield reduced ε_r values that are one order of magnitude smaller than bulk values.[7,8] This size-effect issue impedes the progress of future MLCC technologies.

Such a problem is clearly observed in thin-film nanocapacitors. The nanocapacitors based on $BaTiO_3$ and related oxides yield reduced ε_r values that are 2–3 orders of magnitude smaller than bulk values.[9–14] Owing to the rather complex compositional and structural aspects of these high-*k* materials, current methods such as chemical vapor deposition (CVD), atomic layer deposition (ALD), metal organic chemical vapor deposition (MOCVD), and the sol–gel process often suffer from the inhomogeneity of composition and crystal structure, which is crucial to high-*k* dielectric thin layers. Furthermore, these techniques generally require elaborate deposition processes with high-temperature annealing, producing undesirable interface reactions and/or thermal strain between the high-*k* layers and the electrodes.[6,15] This "dead-layer" problem results in greatly degraded ε_r of high-*k* thin films.[16]

Toward overcoming these issues, nanocrystal technology is an emerging research area with the goal of using nanomaterials as core device components. A unique strategy involving layer-by-layer deposition of high-*k* oxide nanosheets has opened up a novel route for this challenge.[17] Oxide nanosheets are molecularly thin two-dimensional (2D) crystals, derived from a layered compound via exfoliation.[18–20] They have a material-dependent unique thickness of 1–2 nm; the chemical compositions and atomic arrangements of host layers are preserved in the exfoliated nanosheets. Recently, we have developed high-*k* nanodielectrics based on metal–oxide nanosheets [$Ti_{0.87}O_2$, Ti_2NbO_7, $(Ca,Sr)_2Nb_3O_{10}$].[17,21–23] Newly developed nanosheets exhibited the highest permittivity ($\varepsilon_r > 100$) ever realized in all known dielectrics in the ultrathin region (<10 nm). The main advantage of 2D nanosheets is their molecularly small thickness, surpassing structures attainable by down-sizing approaches. 2D nanosheets may therefore be suitable for the miniaturization in capacitor devices.

Here, we review the progress made in dielectric nanosheets, highlighting emerging functionalities in capacitor applications. We also present a perspective on the advantages offered by this class of materials for capacitor applications.

2. 2D dielectric nanosheets

Recently, a variety of oxide nanosheets have been synthesized by delaminating the precursors of layered oxides into their elemental layers.[20,24] These oxide nanosheets have distinct differences and advantages compared with graphene and other 2D materials because of their potential use as insulators, semiconductors, and even conductors, depending on their chemical composition and structures of the parent layered compounds.[25] Oxide nanosheets thus present a tantalizing prospect of scaling all electronic technology down to a truly atomic scale.

Most oxide nanosheets synthesized so far are d^0 transition metal oxides (with Ti^{4+}, Nb^{5+}, Ta^{5+}, and W^{6+}) with insulating and wide-gap semiconducting nature.[17,25] Such d^0 oxide nanosheets can thus be utilized as high-*k* nanodielectrics. Despite significant advances in graphene-like 2D nanosheets, it remains a challenge to explore high-*k* dielectric counterparts, which have great potential in new 2D electronics. Oxide nanosheets may be the perfect solution as a new era unfolds in 2D dielectrics.

$Ti_{0.87}O_2$ is the first example of dielectric nanosheets that represent a modification of nanometer-sized titanium oxide prepared by delaminating a layered titanate into single sheets (Fig. 1).[18,19] $Ti_{0.87}O_2$ nanosheet is composed of only TiO_6 octahedra, a key building block for Ti-based dielectrics, and can thus be viewed as an ideal base for high-*k* dielectrics with a critical thickness. Theoretical and experimental investigations have demonstrated that $Ti_{0.87}O_2$ nanosheet acts as a

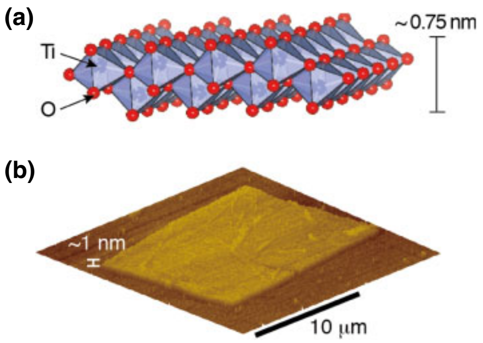

Fig. 1. (Color online) High-k titania nanosheet. (a) Structure model of $Ti_{0.87}O_2$ nanosheet. The Ti atom is coordinated with six oxygen atoms and the resulting TiO_6 octahedra are joined via edge-sharing to produce the 2D lattice. Its thickness is ~0.75 nm, consisting of two edge-shared TiO_6 octahedra. (b) AFM image of $Ti_{0.87}O_2$ nanosheet supported on a SiO_2/Si substrate. Adapted from Ref. 30.

high-k nanoblock, and its multilayer films exhibit both high dielectric constant ($\varepsilon_r = 125$) and highly insulating properties at thicknesses down to 10 nm.[21,26,27] Such a highly insulating nature is attributed to the wide-bandgap nature of $Ti_{0.87}O_2$ nanosheets.[28–30] In bulk TiO_2, anatase and rutile forms possess much smaller bandgaps of 3.2 and 3.0 eV, respectively. Also, bulk TiO_2 often suffers from the well-known problem of oxygen vacancies; the thin films in the anatase and rutile forms have many oxygen vacancies, which causes high leakage density. $Ti_{0.87}O_2$ nanosheets possess Ti vacancies; oxygen vacancies are not expected in this system. Also, owing to quantum confinement effects, 2D nanosheets have an enlarged bandgap,[31] which are favorable for realizing a highly insulating nature.

Perovskite nanosheets form the basis of interesting classes of dielectric materials.[26] The exfoliation of layered perovskites has been reported for Dion–Jacobson phases including $LaNb_2O_7$, $(Ca,Sr)_2Nb_3O_{10}$, $CaLaNb_2TiO_{10}$, $La_2Ti_2NbO_{10}$,[32–35] and for some other materials with Ruddlesden–Popper ($SrLaTi_2TaO_{10}$, $Ca_2Ta_2TiO_{10}$)[33] and Aurivillius ($SrBi_2Ta_2O_9$, $Bi_4Ti_3O_{12}$) phases.[36,37] An important aspect is that these nanosheets consist of perovskite building blocks of TiO_6, NbO_6, or TaO_6 octahedra with a high molecular polarizability.[22,38] $Ca_2Nb_3O_{10}$ nanosheets have extensively been investigated as high-k nanodielectrics [Fig. 2(a)]; their multilayer films exhibited high permittivity ($\varepsilon_r > 200$) and insulating properties even at a nanoscale thicknesses of 5–20 nm.

Current research on these high-k nanosheets is directed toward materials design with tailored composition and structure, and improving their high-k performance. In bulk high-k systems, various strategies have been developed for designing new high-k dielectrics, either by doping more polarizable ions into the lattice or tuning the structural distortion. Such a site-engineering technique is indeed useful for designing dielectric properties in perovskite nanosheets.[22,39–41] In this context, the composition of oxide nanosheets can be intentionally modified by using designated layered compounds; the chemical compositions and atomic arrangements of the host layers are preserved in the exfoliated nanosheets. In perovskite nanosheets ($Ca_{2-x}Sr_xNb_{3-y}Ta_yO_{10}$), A- and B-site modifications may control the polarizability of the octahedra, allowing for the tuning of dielectric responses

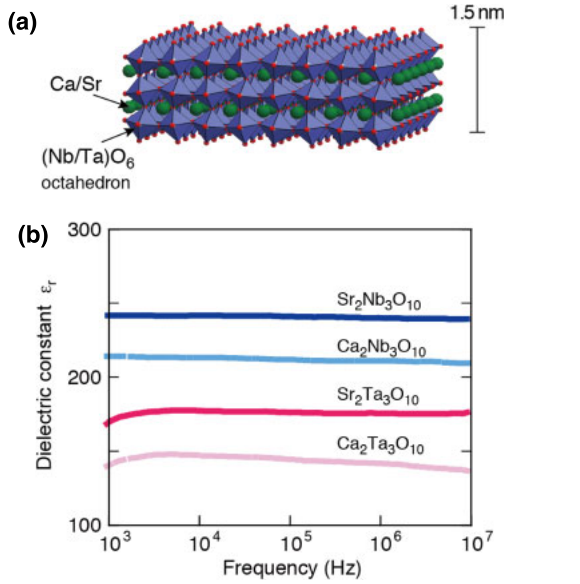

Fig. 2. (Color online) High-k perovskite nanosheets. (a) A- and B-site modifications in $Ca_2Nb_3O_{10}$ nanosheet. (b) Frequency dependence of ε_r for 5-layer films of perovskite nanosheets ($Ca_2Nb_3O_{10}$, $Sr_2Nb_3O_{10}$, $Ca_2Ta_3O_{10}$, and $Sr_2Ta_3O_{10}$). Adapted from Ref. 17. © 2012 John Wiley & Sons, Inc.

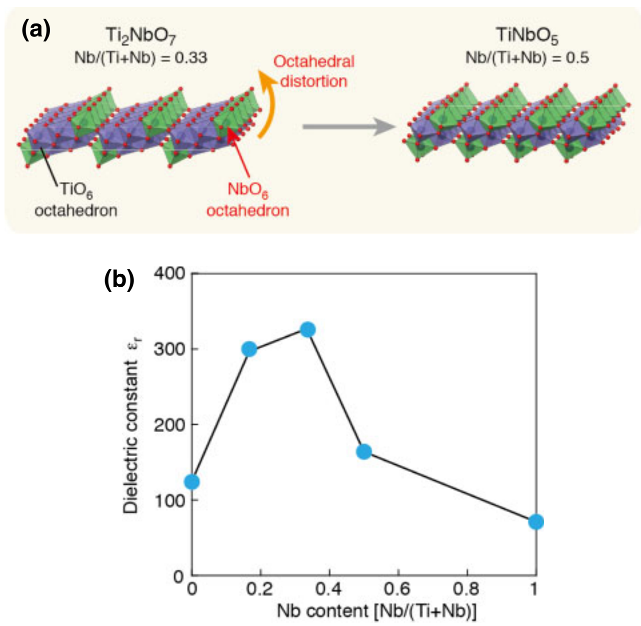

Fig. 3. (Color online) Titano-niobate nanosheets. (a) Structural modification of titano-niobate nanosheets ($Ti_{0.87}O_2$, Ti_2NbO_7, and $TiNbO_5$). (b) Composition dependence of ε_r for 10-layer films of $TiNbO_5$, Ti_2NbO_7, Ti_5NbO_{14}, $Ti_{0.87}O_2$, and Nb_3O_8 nanosheets. Adapted from Ref. 23. © 2012 John Wiley & Sons, Inc.

[Fig. 2(b)].[22,41] In $Ca_2Nb_3O_{10}$ nanosheets, for example, A-site modification with Sr^{2+} ions increased ε_r, whereas B-site modification with Ta^{5+} ions improved leakage current characteristics and reduced ε_r. The optimum property ($\varepsilon_r = 240$) was obtained for $Sr_2Nb_3O_{10}$ nanosheets.

Even elegant materials design can be achieved in titano-niobate nanosheets ($TiNbO_5$, Ti_2NbO_7, Ti_5NbO_{14}) (Fig. 3).[23] In these nanosheets, the octahedral distortion inherent to site engineering by Nb incorporation resulted in a very high molecular polarizability, and their multilayer nanofilms exhibited high ε_r values (160–320) with low leakage current

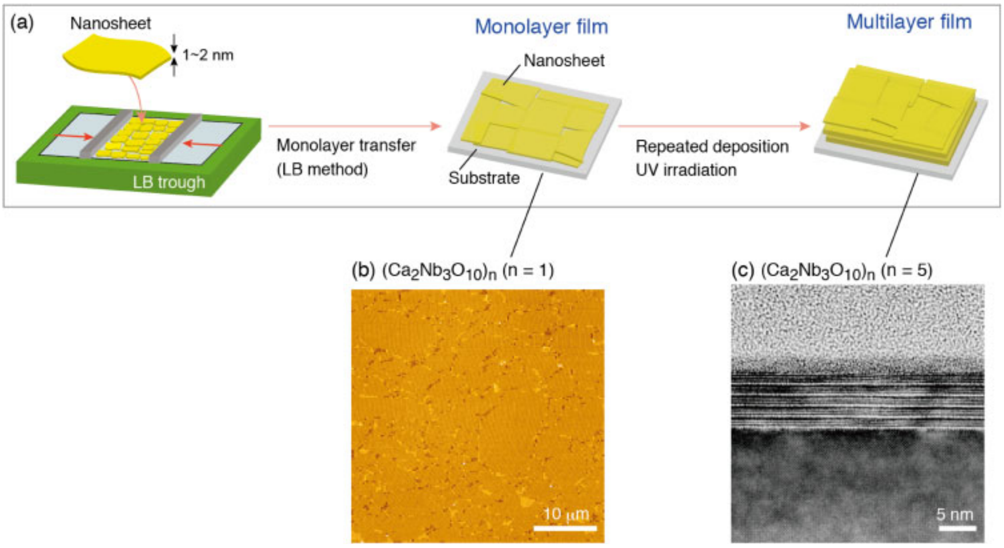

Fig. 4. (Color online) (a) Fabrication procedure for the multilayer nanosheet films using the LB method. (b) AFM image of $Ca_2Nb_3O_{10}$ nanosheets. (c) Cross-sectional high-resolution TEM image of 5-layer films of $Ca_2Nb_3O_{10}$ nanosheets.

densities ($<10^{-7}$ A/cm^2). The optimized property was observed in Ti_2NbO_7 [Nb/(Ti + Nb) = 0.33], in which ε_r reached ∼320, the highest value realized in all known dielectrics in the ultrathin region (<10 nm).

3. Nanosheet-based capacitors

The unique features of 2D nanosheets make them important and fascinating research targets for capacitor applications. Considering the well-known relationship $C = \varepsilon_0 \varepsilon_r S/d$, oxide nanosheets are good capacitor materials, affording a high capacitor density due to their high permittivity and molecular thickness.

In the course of developing capacitor applications, current research is now directed toward the assembly of high-*k* nanosheets into nanostructured films.[17] An important and attractive aspect in this regard is that oxide nanosheets can be obtained as negatively charged crystallites that are dispersed in a colloidal suspension. Oxide nanosheets can be organized into ultrathin films by applying solution-based layer-by-layer assembly such as sequential adsorption deposition[42,43] and Langmuir–Blodgett (LB) deposition.[44,45] LB deposition has been proven to be the most effective approach for organizing 2D nanosheets (Fig. 4). In LB deposition, a floating monolayer of nanosheets is formed on a water surface in a LB trough followed by an appropriate level of compression; the packing density of the nanosheets in the film could be controlled via the surface pressure of the air-water interface. The resulting monolayer films were characterized by well-ordered arrangements of nanosheets with only occasional overlaps and gaps. Nearly perfect mono- and multilayer films have been achieved on the atomically flat conducting substrates such as $SrTiO_3$:Nb, $SrRuO_3$, and Pt.[17] An advantage of this approach is the experimental realization of the atomically sharp interface between the nanosheets and the substrate. Figure 5 shows a cross-sectional high-resolution TEM image of a typical perovskite nanocapacitor [$Au/(Ca_2Nb_3O_{10})_n/SrRuO_3$].[46] Clearly, there were no detectable interdiffusion and strains at the interface, suggesting the production of a dead-layer-free perovskite superlattice directly assembled on the substrate.

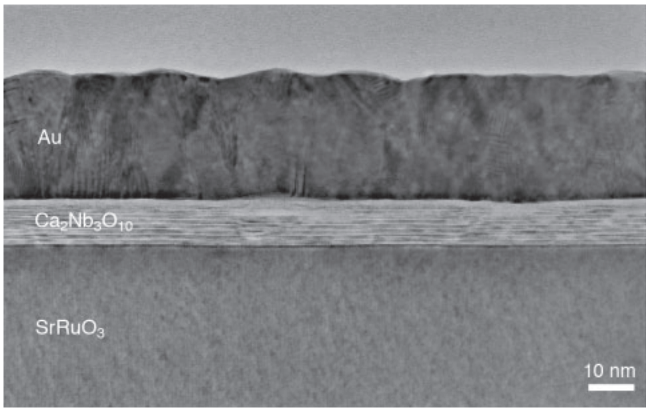

Fig. 5. High-resolution TEM image of a $Au/(Ca_2Nb_3O_{10})_n/SrRuO_3$ nanocapacitor ($n = 10$). Adapted from Ref. 46. © 2014 American Chemical Society.

Reflecting its highly organized structure, the nanosheet films show superior dielectric and insulating properties.[17,21–23] A common feature of the nanosheet films is the size-effect-free characteristic of dielectric responses; the multilayer films of $Ti_{0.87}O_2$, Ti_2NbO_7, and $(Ca,Sr)_2Nb_3O_{10}$ nanosheets showed stable dielectric responses even down to a thickness of 10 nm. In the $Ca_2Nb_3O_{10}$ case, the multilayer films maintained a constant ε_r value of ∼210 irrespective of the film thickness, where the dielectric loss ($\tan\delta$) was ∼2–5%.[22] These $(Ca_2Nb_3O_{10})_n$ films also exhibited excellent insulating characteristics; the dielectric breakdown occurred at 3–4 MV/cm. Figure 6 summarizes the ε_r values of perovskite nanosheets and various perovskite thin films. In the ultrathin region (<20 nm), the ε_r values of perovskite nanosheets were higher than those of the other perovskites. In $Sr_2Nb_3O_{10}$ and $Ca_2Nb_3O_{10}$, ε_r reached >200, which is 10 times larger than that of $(Ba_{1-x}Sr_x)TiO_3$ films of the same thickness. The high ε_r values of perovskite nanosheets persisted even in the <10 nm region, which is in sharp contrast to the size-induced dielectric collapse in $(Ba_{1-x}Sr_x)TiO_3$.[11,13,14] These results suggest that perovskite nanosheets are very promising candidates for high-density capacitor applications.

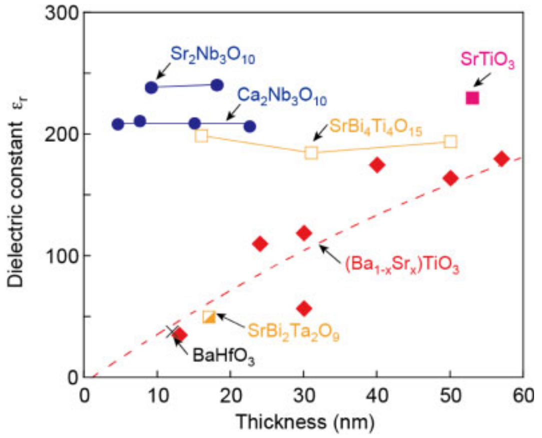

Fig. 6. (Color online) ε_r for perovskite nanosheets and various perovskite thin films. Adapted from Ref. 17. © 2012 John Wiley & Sons, Inc.

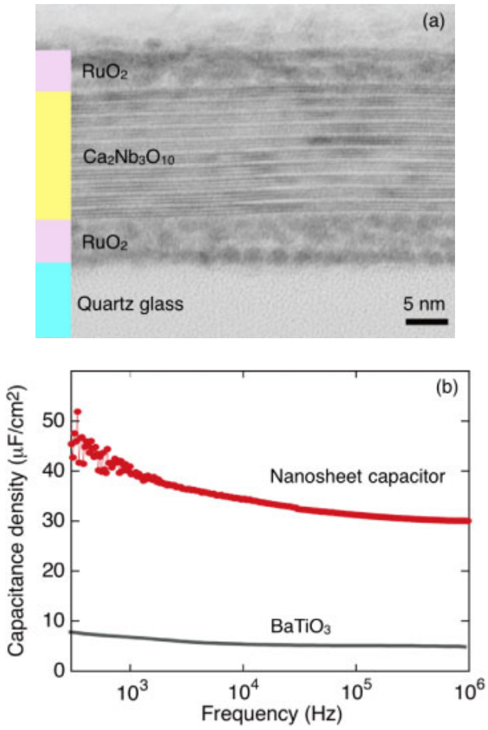

Fig. 7. (Color online) (a) High-resolution TEM image and (b) dielectric property of a $(Ru_{0.95}O_2)_5/(Ca_2Nb_3O_{10})_{10}/(Ru_{0.95}O_2)_5$ nanosheet capacitor. In (b), the dielectric property of $BaTiO_3$ is also included.

Considering these aspects, the sequential organization of metallic and dielectric nanosheet films into a sandwich structure would be a powerful approach to constructing all-nanosheet ultrathin capacitors. This approach enables the reduction in thickness in both the dielectric and electrode layers, which provides an ultimate route for designing ultrathin capacitors. Recently, all-nanosheet capacitors have been successfully fabricated by layer-by-layer assembly using two types of oxide nanosheets (Fig. 7).[47] One is $Ru_{0.95}O_2$ for top and bottom electrodes and the other is $Ca_2Nb_3O_{10}$ for the dielectric layer. Even with the small thickness of 28 nm, the system actually worked as an ultrathin capacitor, achieving a high capacitance density (~30 μF/cm^2). The obtained capacitance density is nearly 10 times that of state-of-the-art HfO_2-based ultrathin capacitors (~0.89 μF/cm^2/10 nm)[48] and approximately 2000 times higher than that of commercial $BaTiO_3$-based capacitors (~20 μF/cm^2/5 × 10^4 nm).[49] This prototype capacitor has a MIM structure (one unit of MLCC), and the multilayer structuring becomes the future challenge.

4. High-temperature applications

The development of high-temperature electronics has been a significant challenge in recent years. For example, automotive industries require electronic components operable at high temperatures (>200 °C). In the capacitor components, however, the absence of suitable materials is one of the major barriers to meeting this goal. $BaTiO_3$ has been widely used in capacitor applications for many years. However, $BaTiO_3$ suffers from a low Curie temperature (T_C) of ~130 °C; a sharp decrease in ε_r above T_C intrinsically limits the use of $BaTiO_3$-based materials in high-temperature environments >200 °C. Various strategies have been developed for tailoring the thermal stability of $BaTiO_3$ and related perovskites. In $BaTiO_3$, chemical modification by doping or using solid solutions is an effective approach to obtaining a broadened dielectric peak while maintaining a high ε_r value.[3,50–53] Another approach is the use of non-polar characteristic of layered ferroelectric materials having high T_C (e.g., $CaBi_4Ti_4O_{15}$ and $SrBi_4Ti_4O_{15}$).[54,55] In future electronics, the requirements for capacitor devices generally tend towards miniaturized dielectrics with higher ε_r, lower loss, and reduced leakage current. The development of new high-temperature nanodielectrics to fulfill these requirements is an important issue but most challenging.

Oxide nanosheets are a fascinating target for such high-temperature applications. Most of the oxide nanosheets [$Ti_{0.87}O_2$, Ti_2NbO_7, $(Ca,Sr)_2Nb_3O_{10}$] are paraelectric, thus yielding a very small temperature coefficient (τ), in contrast to the large variation of ferroelectric materials. Another important aspect of oxide nanosheets is their thermal stability. In $Ca_2Nb_3O_{10}$, the 2D perovskite structure was stable up to 700 °C in a monolayer film with an extremely small thickness of ~2 nm.[56] Various in situ characterizations revealed a robust thermal stability of insulating behavior even in monolayer $Ca_2Nb_3O_{10}$ films, and layer-by-layer assembled nanocapacitors exhibited stable dielectric and insulating responses up to 250 °C (Fig. 8).[46] Perovskite nanosheets also offer a unique opportunity for tailoring the temperature dependence through doping and lattice engineering. Perovskite nanosheets yielded a very small temperature coefficient (τ), which is much smaller than those of typical high-*k* dielectrics (>−1,000 ppm/K for $Ba_{1-x}Sr_xTiO_3$). In $Ca_{2-x}Sr_xNb_{3-y}Ta_yO_{10}$, the overall trend varied from negative values (−210 ppm/K) in Ca-based nanosheets ($Ca_2Ta_3O_{10}$) to positive values (+150, +180 ppm/K) in Sr-based nanosheets ($Sr_2Nb_3O_{10}$, $Sr_2Ta_3O_{10}$) in the temperature range of −25 to +150 °C.[22,41] The opposite signs of Ca- and Sr-based nanosheets offer the tantalizing possibility that solid solutions could be formed with high ε_r values and near-zero τ. The simultaneous improvements in the ε_r, τ, and J properties observed in the ultrathin forms of single-phase materials are desirable for many capacitor applications,[57] and perovskite nanosheets have great potential for a rational design and construction of high-temperature capacitor devices.

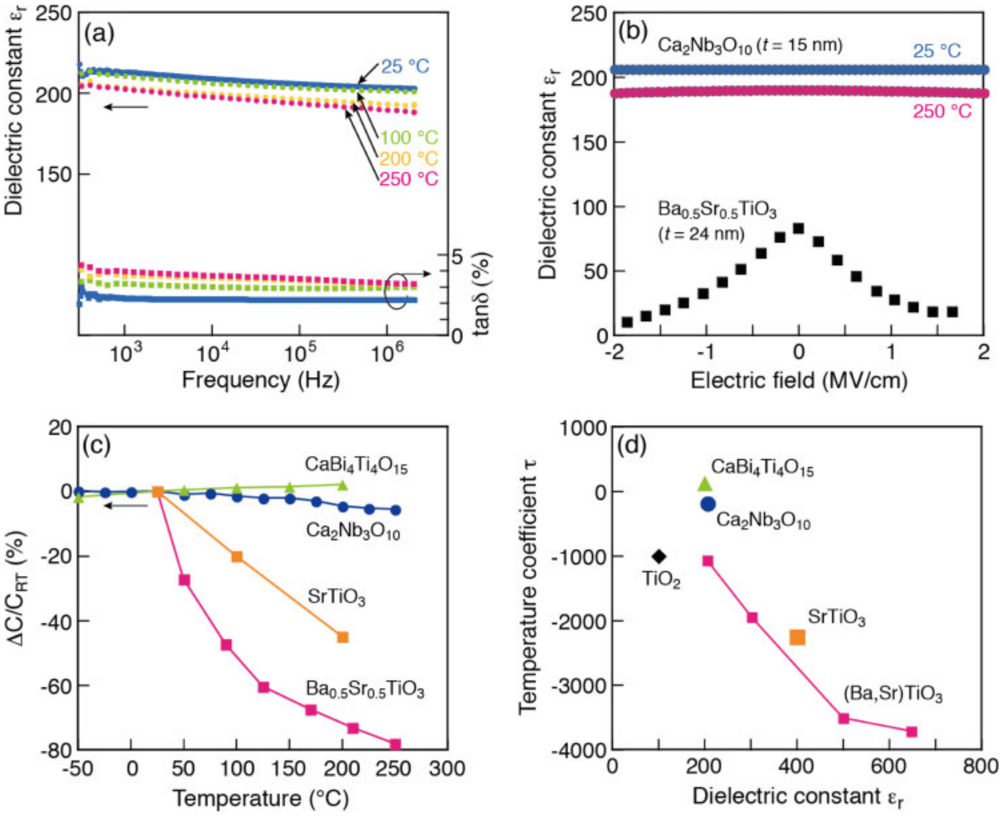

Fig. 8. (Color online) (a) Frequency dependence of the ε_r and tan δ of a Au/$(Ca_2Nb_3O_{10})_n$/$SrRuO_3$ ($n = 10$) nanocapacitor at 25, 100, 200, and 250 °C. (b) ε_r–V curves measured at 25 and 250 °C for the same nanocapacitor as in Fig. 3(a). The frequency was 10 kHz. The data of $Ba_{0.5}Sr_{0.5}TiO_3$ (25 °C, $t = 24$ nm) are also included for a comparison. (c) Temperature dependence of the capacitance change relative to RT value ($\Delta C/C_{RT}$) for $Ca_2Nb_3O_{10}$ nanosheets and perovskite thin films. (d) Plot of the temperature coefficients (τ) for $Ca_2Nb_3O_{10}$ nanosheets and perovskite thin films. Adapted from Ref. 46. © 2014 American Chemical Society.

5. Conclusion

We have reviewed the current status of research on 2D dielectric nanosheets. Recently, a variety of oxide nanosheets have been synthesized, and their unique dielectric properties have been investigated. Newly developed nanosheets [$Ti_{0.87}O_2$, Ti_2NbO_7, $(Ca,Sr)_2Nb_3O_{10}$] exhibited the highest permittivity ($\varepsilon_r > 100$) ever realized in all known dielectrics in the ultrathin region (<10 nm). The main advantage of 2D nanosheets is their molecular-thin thickness, surpassing structures attainable by down-sizing approaches. 2D nanosheet may therefore be suitable for the miniaturization of capacitor devices. Nanosheet-based capacitors retained their size-free high-ε_r characteristic and high insulation resistance with high breakdown voltages at high temperatures up to 250 °C. They also exhibited small τ values, offering a performance superior to current high-k materials. Since $Ca_2Nb_3O_{10}$ nanosheets possess a robust thermal stability up to 700 °C, the optimization of device structures would facilitate their use at much higher temperatures (even at 500 °C). In addition, perovskite nanosheets are Pb-free and RoHS compliant, which are a key issue for future electronics.

Although nanosheet technology has great potentials for future electronics, there remain many issues to be solved for the practical applications. The first issue is the choice of electrodes. In our works, nanosheet capacitors have been tested mostly on atomically flat substrates to highlight the best performance. The test has not confirmed any critical aspect on common, large-scale electrodes under downgraded conditions. The second issue is reliability. High-temperature applications are specific for their harsh electrical and environmental conditions together with requirements for high overall reliability and long lifetime. Any electronic components used in such applications play important roles to ensure reliability and functionality. Furthermore, the absence of reliable fabrication methods for large-scale devices of 3D structures is one of the main hurdles. However, there are promising signs that these problems will soon be overcome. Concerning fabrication, a solution-based process at room temperature has great advantages when developing large-scale manufacturing processes. The fabrication process involving layer-by-layer assembly of nanosheets without costly fabrication lines and special annealing processes for metal electrode layers is another great advantage particularly in practical applications for various capacitors; there are no strict limitations on the dimensions, shapes, and materials of substrates. Furthermore, all-nanosheet capacitors may be readily assembled on plastic or flexible substrates.

This review focused on capacitor applications. Oxide nanosheets are also of technological importance for establishing dielectrics on 2D materials, which have great potentials in various electronic applications such as energy storages,[17] gate devices,[25,58] and ferroelectrics/multiferroics.[59–62]

Acknowledgments

The authors are grateful to Dr. Y. Ebina, Dr. R. Ma, Dr. T. C. Ozawa, Dr. B.-W. Li, Dr. K. Akatsuka, Dr. Y.-H. Kim (NIMS), Professor H. Funakubo (TIT), Professor W.

Sugimoto (Shinshu University), Dr. K. Fukuda (Kyoto University), and Professor K. Ono (KEK) for their contribution in experiments and stimulating discussions over the years of the authors' research on oxide nanosheets. This work was in part supported by World Premier International Research Center Initiative (WPI Initiative on Materials Nanoarchitronics), MEXT, CREST, JST, and a Grant-in-Aid for Scientific Research, MEXT, Japan.

1) Y. Sakabe, Curr. Opin. Solid State Mater. Sci. **2**, 584 (1997).
2) C. A. Randall, J. Ceram. Soc. Jpn. **109**, S2 (2001).
3) H. Kishi, Y. Mizuno, and H. Chazono, Jpn. J. Appl. Phys. **42**, 1 (2003).
4) C. Pithan, D. Hennings, and R. Waser, Int. J. Appl. Ceram. Technol. **2**, 1 (2005).
5) C. A. Mead, Phys. Rev. Lett. **6**, 545 (1961).
6) M. Stengel and N. A. Spaldin, Nature **443**, 679 (2006).
7) M. H. Frey and D. A. Payne, Phys. Rev. B **54**, 3158 (1996).
8) J. Petzelt, Ferroelectrics **400**, 117 (2010).
9) C. S. Hwang, S. O. Park, H. J. Cho, C. S. Kang, H. K. Kang, S. I. Lee, and M. Y. Lee, Appl. Phys. Lett. **67**, 2819 (1995).
10) C. Zhou and D. M. Newns, J. Appl. Phys. **82**, 3081 (1997).
11) P. Padmini, T. R. Taylor, M. J. Lefevre, A. S. Nagra, R. A. York, and J. S. Speck, Appl. Phys. Lett. **75**, 3186 (1999).
12) V. Craciun and R. K. Singh, Appl. Phys. Lett. **76**, 1932 (2000).
13) M. C. Werner, I. Banerjee, P. C. McIntyre, N. Tani, and M. Tanimura, Appl. Phys. Lett. **77**, 1209 (2000).
14) C. S. Hwang, J. Appl. Phys. **92**, 432 (2002).
15) L. W. Chang, M. McMillen, F. D. Morrison, J. F. Scott, and J. M. Gregg, Appl. Phys. Lett. **93**, 132904 (2008).
16) L. W. Chang, M. Alexe, J. F. Scott, and J. M. Gregg, Adv. Mater. **21**, 4911 (2009).
17) M. Osada and T. Sasaki, Adv. Mater. **24**, 210 (2012).
18) T. Sasaki, M. Watanabe, H. Hashizume, H. Yamada, and H. Nakazawa, J. Am. Chem. Soc. **118**, 8329 (1996).
19) T. Sasaki and M. Watanabe, J. Am. Chem. Soc. **120**, 4682 (1998).
20) R. Z. Ma and T. Sasaki, Adv. Mater. **22**, 5082 (2010).
21) M. Osada, Y. Ebina, H. Funakubo, S. Yokoyama, T. Kiguchi, K. Takada, and T. Sasaki, Adv. Mater. **18**, 1023 (2006).
22) M. Osada, K. Akatsuka, Y. Ebina, H. Funakubo, K. Ono, K. Takada, and T. Sasaki, ACS Nano **4**, 5225 (2010).
23) M. Osada, G. Takanashi, B.-W. Li, K. Akatsuka, Y. Ebina, K. Ono, H. Funakubo, K. Takada, and T. Sasaki, Adv. Funct. Mater. **21**, 3482 (2011).
24) L. Wang and T. Sasaki, Chem. Rev. **114**, 9455 (2014).
25) M. Osada and T. Sasaki, J. Mater. Chem. **19**, 2503 (2009).
26) H. Sato, K. Ono, T. Sasaki, and A. Yamagishi, J. Phys. Chem. B **107**, 9824 (2003).
27) M. Osada, K. Akatsuka, Y. Ebina, Y. Kotani, K. Ono, H. Funakubo, S. Ueda, K. Kobayashi, K. Takada, and T. Sasaki, Jpn. J. Appl. Phys. **47**, 7556 (2008).
28) T. Sasaki and M. Watanabe, J. Phys. Chem. B **101**, 10159 (1997).
29) Y.-H. Kim, M. Osada, L. Dong, H.-J. Kim, and T. Sasaki, J. Ceram. Soc. Jpn. **123**, 335 (2015).
30) H.-J. Kim, M. Osada, Y. Ebina, W. Sugimoto, K. Tsukagoshi, and T. Sasaki, Sci. Rep. **6**, 19402 (2016).
31) N. Sakai, Y. Ebina, K. Takada, and T. Sasaki, J. Am. Chem. Soc. **126**, 5851 (2004).
32) Y. Ebina, K. Akatsuka, K. Fukuda, and T. Sasaki, Chem. Mater. **24**, 4201 (2012).
33) R. E. Schaak and T. E. Mallouk, Chem. Mater. **14**, 1455 (2002).
34) Y. Ebina, T. Sasaki, and M. Watanabe, Solid State Ionics **151**, 177 (2002).
35) T. C. Ozawa, K. Fukuda, K. Akatsuka, Y. Ebina, and T. Sasaki, Chem. Mater. **19**, 6575 (2007).
36) S. Ida, C. Ogata, U. Unal, K. Izawa, T. Inoue, O. Altuntasoglu, and Y. Matsumoto, J. Am. Chem. Soc. **129**, 8956 (2007).
37) J. Y. Kim, I. Chung, J. H. Choy, and G. S. Park, Chem. Mater. **13**, 2759 (2001).
38) B.-W. Li, M. Osada, Y. Ebina, T. C. Ozawa, R. Ma, and T. Sasaki, Appl. Phys. Lett. **96**, 182903 (2010).
39) B.-W. Li, M. Osada, T. C. Ozawa, R. Ma, K. Akatsuka, Y. Ebina, H. Funakubo, S. Ueda, K. Kobayashi, and T. Sasaki, Jpn. J. Appl. Phys. **48**, 09KA15 (2009).
40) B.-W. Li, M. Osada, T. C. Ozawa, K. Akatsuka, Y. Ebina, R. Ma, K. Ono, H. Funakubo, and T. Sasaki, Jpn. J. Appl. Phys. **49**, 09MA01 (2010).
41) M. Osada and T. Sasaki, Int. J. Appl. Ceram. Technol. **9**, 29 (2012).
42) T. Sasaki, Y. Ebina, T. Tanaka, M. Harada, M. Watanabe, and G. Decher, Chem. Mater. **13**, 4661 (2001).
43) T. Tanaka, K. Fukuda, Y. Ebina, K. Takada, and T. Sasaki, Adv. Mater. **16**, 872 (2004).
44) M. Muramatsu, K. Akatsuka, Y. Ebina, K. Wang, T. Sasaki, T. Ishida, K. Miyake, and M. Haga, Langmuir **21**, 6590 (2005).
45) K. Akatsuka, M. Haga, Y. Ebina, M. Osada, K. Fukuda, and T. Sasaki, ACS Nano **3**, 1097 (2009).
46) Y.-H. Kim, H.-J. Kim, M. Osada, B. W. Li, Y. Ebina, and T. Sasaki, ACS Appl. Mater. Interfaces **6**, 19510 (2014).
47) C. Wang, M. Osada, Y. Ebina, B.-W. Li, K. Akatsuka, K. Fukuda, W. Sugimoto, R. Ma, and T. Sasaki, ACS Nano **8**, 2658 (2014).
48) V. K. Sangwan, D. Jariwala, S. A. Filippone, H. J. Karmel, J. E. Johns, J. M. P. Alaboson, T. J. Marks, L. J. Lauhon, and M. C. Hersam, Nano Lett. **13**, 1162 (2013).
49) Web [http://www.murata.com/new/news_release/2009/1005b/index.html].
50) D. Hennings, A. Schnell, and G. Simon, J. Am. Ceram. Soc. **65**, 539 (1982).
51) J. B. Lim, S. Zhang, N. Kim, and T. R. Shrout, J. Am. Ceram. Soc. **92**, 679 (2009).
52) W. Xiaoyong, F. Yujun, and Y. Xi, Appl. Phys. Lett. **83**, 2031 (2003).
53) R. Dittmer, W. Jo, D. Damjanovic, and J. Rödel, J. Appl. Phys. **109**, 034107 (2011).
54) K. Takahashi, M. Suzuki, T. Kojima, T. Watanabe, Y. Sakashita, K. Kato, O. Sakata, K. Sumitani, and H. Funakubo, Appl. Phys. Lett. **89**, 082901 (2006).
55) J. Kimura, I. Takuwa, M. Matsushima, S. Yasui, T. Yamada, and H. Funakubo, J. Appl. Phys. **114**, 027002 (2013).
56) B.-W. Li, M. Osada, Y. Ebina, K. Akatsuka, K. Fukuda, and T. Sasaki, ACS Nano **8**, 5449 (2014).
57) R. J. Cava, J. Mater. Chem. **11**, 54 (2001).
58) W. Li, S.-L. Li, K. Komatsu, A. Aparecido-Ferreira, Y.-F. Lin, Y. Xu, M. Osada, T. Sasaki, and K. Tsukagoshi, Appl. Phys. Lett. **103**, 023113 (2013).
59) B.-W. Li, M. Osada, T. C. Ozawa, Y. Ebina, K. Akatsuka, R. Ma, H. Funakubo, and T. Sasaki, ACS Nano **4**, 6673 (2010).
60) B.-W. Li, M. Osada, K. Akatsuka, Y. Ebina, T. C. Ozawa, and T. Sasaki, Jpn. J. Appl. Phys. **50**, 09NA10 (2011).
61) Y.-H. Kim, L. Dong, M. Osada, B.-W. Li, Y. Ebina, and T. Sasaki, Nanotechnology **26**, 244001 (2015).
62) B.-W. Li, M. Osada, Y. Ebina, S. Ueda, and T. Sasaki, J. Am. Chem. Soc. **138**, 7621 (2016).